

Research Article

# Pyran-annulated derivatives synthesized via multi-component reactions as multi-target agents with anti-inflammatory, anti-melanogenesis, and anti-cancer activities

Dina Nur Shinta<sup>a</sup>, Ardiansah Ardiansah<sup>a</sup>, Siwattra Choodej<sup>b</sup>, Natthaya Chuaypen<sup>c</sup>, Khanitha Pudhom<sup>a,\*</sup>

<sup>a</sup>Department of Chemistry, Chulalongkorn University, Payatai Rd., Wongmai, Patumwan, 10330, Thailand

<sup>b</sup>Department of Chemistry, Faculty of Science, King Mongkut's University of Technology Thonburi, Pracha Uthit Rd., Bang Mod, Thung Khru, 10140, Bangkok, Thailand

<sup>c</sup>Department of Biochemistry, Faculty of Medicine, Chulalongkorn University, Payatai Rd., Patumwan, 10330, Thailand

## ARTICLE INFO

### Keywords:

Anti-cancer  
Anti-inflammation  
Anti-melanogenesis  
Multi-target bioactivity  
Pyran-annulated derivatives

## ABSTRACT

Pyran-annulated derivatives are multifunctional scaffolds that exhibit diverse biological activities, including anti-inflammatory, anti-melanogenesis, and anti-cancer effects. This study aimed to synthesize a series of pyran-annulated derivatives and evaluate their biological properties *in vitro*, to identify potential multi-target therapeutic candidates. The synthesized compounds were screened for anti-inflammatory activity by measuring nitric oxide (NO) inhibition in lipopolysaccharide (LPS)-stimulated J774A.1 macrophages. Anti-melanogenesis activity was evaluated in B16F10 melanoma cells, while cytotoxicity was assessed against MDA-MB-231 triple-negative breast cancer cells. Western blot assays were conducted to examine the expression of inflammation and melanogenesis-related proteins, while molecular docking was performed to investigate binding affinity to the cyclooxygenase-2 (COX-2) active site. In addition, wound-healing assays were carried out to assess the impact of cancer cell migration. Among the tested compounds, A05 emerged as the most active compound, displaying potent multi-target effects. It showed an  $IC_{50}$  value of 10.2  $\mu$ M for NO inhibition, surpassing indomethacin ( $IC_{50}$  = 44.5  $\mu$ M), 13.3  $\mu$ M for melanin inhibition, and 24.3  $\mu$ M for cytotoxicity against MDA-MB-231 cells. Western blot analysis confirmed that A05 significantly downregulated COX-2, iNOS, and TNF- $\alpha$  in J774A.1 macrophages, while suppressing MITF and TRP-1 expression in B16F10 cells. Molecular docking results revealed strong binding of A05 to the COX-2 active site, supporting its anti-inflammatory action. Furthermore, wound-healing assays demonstrated that A05 effectively inhibited cancer cell migration. These findings highlight A05 as a promising lead compound with combined anti-inflammatory, anti-melanogenesis, and anti-cancer properties. Its ability to simultaneously modulate multiple biological pathways underscores its potential as a candidate for the development of multi-target therapeutic agents.

## 1. Introduction

Cancer progression, melanogenesis, and inflammation are interconnected biological processes that share several overlapping molecular pathways. Dysregulated cell proliferation and survival, a hallmark of cancer, are often accompanied by aberrant activation of signaling cascades such as mitogen-activated protein kinase (MAPK) and phosphoinositide 3-kinase/Akt (PI3K/Akt) pathways, which also regulate melanogenesis and inflammatory responses (Stewart *et al.*, 2003; Lee *et al.*, 2021). In melanocytes, the MAPK and PI3K/Akt modulate the expression of microphthalmia-associated transcription factor (MITF), a master regulator of melanogenic enzymes including tyrosinase, thereby influencing melanin production (Bae and Hyun 2023). Similarly, in immune cells, these pathways interact with nuclear factor kappa B (NF- $\kappa$ B) signaling to regulate the expression of pro-inflammatory mediators such as nitric oxide (NO) and cytokines (Cao *et al.*, 2024). Chronic inflammation has been recognized as a critical factor in carcinogenesis, promoting tumor initiation, progression, and metastasis through the generation of reactive oxygen/nitrogen

species and the activation of oncogenic transcription factors (Sung *et al.*, 2021; Thandra *et al.*, 2021). In the tumor microenvironment, inflammatory mediators such as NO not only facilitate angiogenesis and immune evasion but also contribute to oxidative stress, which can dysregulate melanogenic processes in skin cells (Fu *et al.*, 2020). Moreover, excessive melanin production can be triggered by oxidative stress-induced activation of MITF, linking pigmentary disorders with inflammatory and neoplastic conditions (Rajan, 2025). Given these shared molecular mechanisms, compounds capable of modulating key signaling pathways, such as MAPK, PI3K/Akt, and NF- $\kappa$ B, may exert multifunctional bioactivities, including anti-cancer, antimelanogenic, and anti-inflammatory effects.

Heterocyclic compounds represent a cornerstone of medicinal chemistry owing to their broad-spectrum biological activities. Among these, 4H-pyran and pyrazole derivatives have drawn considerable attention for their therapeutic potential. Pyran-annulated heterocycles are widely distributed in natural products and have been reported to exhibit anti-oxidant (Khare *et al.*, 2019), anti-bacterial (Amirnejat *et al.*, 2020), anti-microbial (El-Sayed *et al.*, 2022), and anti-cancer (Cholayil

### \*Corresponding author:

E-mail address: [khanitha.p@chula.ac.th](mailto:khanitha.p@chula.ac.th) (K Pudhom)

Received: 27 August, 2025 Accepted: 18 November, 2025 Epub Ahead of Print: 09 February, 2026 Published: 24 February, 2026

DOI: 10.25259/JKSUS\_1363\_2025

Palapetta et al., 2023). Likewise, benzopyrone-based heterocycles such as coumarins, which are abundant in plants or other organisms, display diverse pharmacological effects, including anti-inflammatory, anti-cancer, anti-coagulant, anti-microbial, and anti-oxidant properties (Kongtogiorgis and Hadjipavlou-Litina, 2005; Borges et al., 2005; Govindaiah et al., 2019; El-Sayed et al., 2022). Given these compelling activities, coumarin was selected as a bioisosteric replacement for the pyrazole moiety within the hybrid 4H-pyran framework to enable comparative evaluation of their biological activities.

In this work, two classes of heterocyclic hybrids, pyrano[2,3-c]pyrazole and pyrano[2,3-c]coumarin derivatives, were synthesized via multi-component reactions (MCRs). This synthetic strategy allows the rapid and efficient assembly of complex fused scaffolds through the one-pot formation of multiple bonds (Ahmad et al., 2023; Selvaraj et al., 2024; Shen et al., 2025; Wang et al., 2023). Beyond their structural novelty, these compounds were evaluated for three interrelated biological activities: their cytotoxicity against MDA-MB-231 breast cancer cell line, their ability to inhibit melanogenesis in B16F10 melanoma cells, and their anti-inflammatory potential in LPS-stimulated macrophages, with particular attention to elucidating their underlying mechanism of action. This integrated approach aims to identify multifunctional agents with potential therapeutic applications in cancer, pigmentation disorders, and inflammation-related pathologies.

## 2. Materials and Methods

### 2.1 Materials and chemicals

All chemicals were purchased from Tokyo Chemical Industry Co., Ltd. (Tokyo, Japan). Thin layer chromatography (TLC) was performed using aluminum plates pre-coated with silica gel (Merck silica gel 60 F-254, 20 × 20 cm, 200 μm). The nuclear magnetic resonance (<sup>1</sup>H and <sup>13</sup>C-NMR) spectra were acquired on a JEOL JNM-ECZ500R/S1 spectrometer operating at 500 MHz for <sup>1</sup>H and 125 MHz for <sup>13</sup>C, with tetramethylsilane (TMS) as the internal reference. Column chromatography (CC) was conducted using silica gel 60 (60–200 μm, Silicycle, Quebec, Canada).

### 2.2 General procedure for synthesis

#### 2.2.1 Pyrano[2,3-c]pyrazoles derivatives (A01-16 and B01-16)

The pyran derivatives were synthesized via a one-pot, stepwise procedure as illustrated in Scheme 1. Initially, hydrazine hydrate or phenyl hydrazine (1.2 eq) was reacted with ethyl acetoacetate (1 eq) at room temperature to afford a C-H-activated intermediate (3-methyl-

pyrazole-5-one or 3-methyl-1-phenyl-pyrazole-5-one) as a white solid. This intermediate was then subjected to a three-component condensation with an aromatic aldehyde (1 eq) and malononitrile (1.2 eq) in the presence of a catalytic amount of 4-dimethylaminopyridine (DMAP) under reflux in ethanol, to yield the corresponding pyrano[2,3-c]pyrazoles derivatives. TLC monitored the completion of the reaction. The products were purified by CC using silica gel with a gradient mixture eluent of hexanes-EtOAc.

#### 2.2.2 Pyrano[2,3-c]coumarins derivatives (C01-12)

The pyranocoumarin derivatives were synthesized via a one-pot, three-component reaction involving 4-hydroxycoumarin (1 eq), various aromatic aldehydes (1 eq), and malononitrile (1.2 eq) in the presence of a catalytic amount of DMAP under reflux in ethanol. The completion of the reaction was monitored by TLC. The final products were obtained as solids and isolated by filtration without further purification.

### 2.3 Biological evaluation

#### 2.3.1 Cell culture

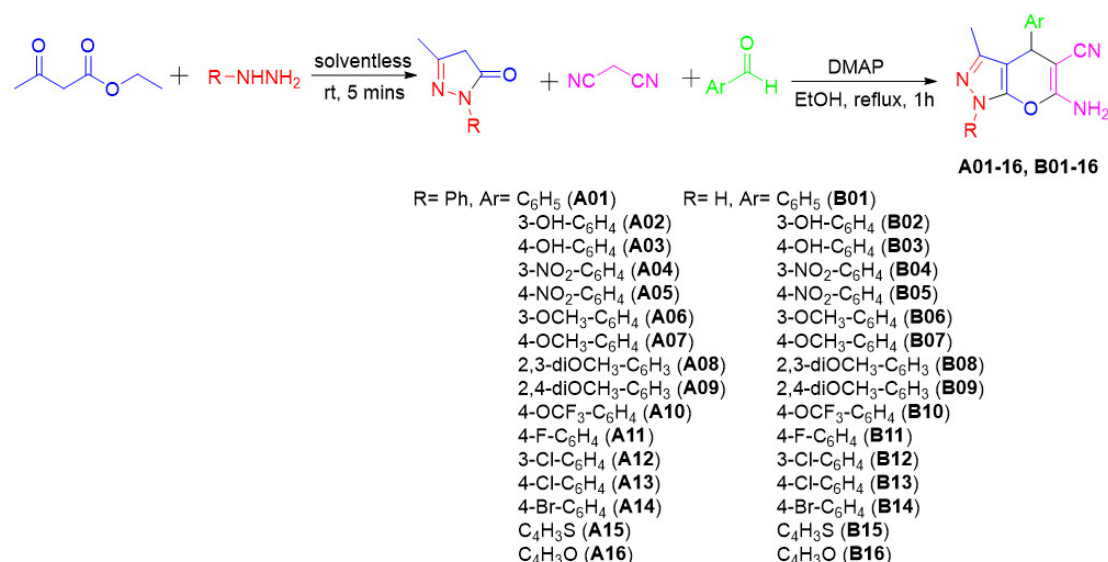
The MDA-MB-231 human breast cancer cell line and the J774A.1 murine macrophage cell line were cultured in dulbecco's modified eagle's medium (DMEM) containing phenol red, while the B16F10 murine melanoma cell line was cultured in DMEM without phenol red. All media were supplemented with 10% fetal bovine serum (FBS), 2 mM L-glutamine, 100 U/mL of penicillin, and 100 mg/mL of streptomycin. Cells were maintained at 37°C in a humidified atmosphere containing 5% CO<sub>2</sub>.

#### 2.3.2 Cytotoxicity against MDA-MB-231 cells

The cytotoxic effects of the compounds on MDA-MB-231 cells were evaluated using the MTT assay. Cells were seeded into a 96-well plate at a density of 5 × 10<sup>3</sup> cells/well in DMEM and incubated for 24 h. Various concentrations of the compounds were then added, and the cells were further incubated for 48 h. Following treatment, MTT solution (5 mg/mL) was added to each well, and the cells were incubated for 4 h. The resulting formazan crystals were dissolved in 100 μL of DMSO, and absorbance was measured at 570 nm using a microplate reader. IC<sub>50</sub> values were calculated using GraphPad Prism™ version 5.

#### 2.3.3 Melanin inhibition in B16F10 cells

B16F10 cells were seeded into a 24-well plate with a density of 5 × 10<sup>4</sup> cells/well and incubated for 24 h. Cells were then treated with



Scheme 1. Synthesis route of pyranopyrazole derivatives (A01-16, B01-16).

various concentrations of the compounds and  $\alpha$ -arbutin (1000  $\mu$ M) as the positive control. After 4 days of treatment, 100  $\mu$ L of culture medium from each well was transferred into a 96-well plate, and absorbance was measured at 510 nm using a microplate reader to determine melanin content. Cell viability was assessed in parallel using the MTT assay as described above.  $IC_{50}$  values were calculated using GraphPad Prism™ version 5.

### 2.3.4 Inhibition of NO in stimulated J774A.1 macrophage cells

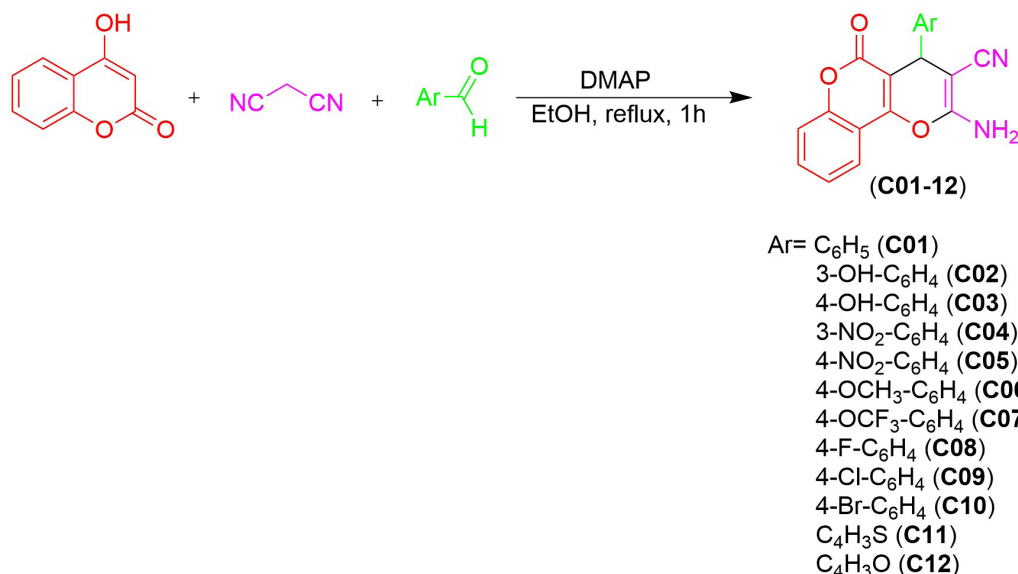
The anti-inflammatory activity of the compounds was determined by their ability to inhibit NO production in LPS-stimulated J774A.1 macrophage cells using the Griess assay, with indomethacin as the positive control. Cells were seeded into a 96-well plate at a density of  $2.5 \times 10^4$  cells/well, and incubated at 37°C in a humidified 5% CO<sub>2</sub> atmosphere for 24 h. Cells were pretreated with various concentrations of the compounds for 2 h, followed by stimulation with LPS (1  $\mu$ g/mL) and further incubation for 20 h. The nitrite concentration in the culture supernatant was quantified using Griess reagent, and absorbance was measured at 540 nm. MTT assay also assessed cytotoxicity.  $IC_{50}$  values were calculated using GraphPad Prism™ version 5.

### 2.3.5 Western blot analysis

Cells were seeded into a 24-well plate at a density of  $2.5 \times 10^5$  cells/well and pretreated with the compounds at various concentrations. Following treatment, cells were washed with cold PBS and lysed using a cell lysis buffer. Lysates were centrifuged at 5000 rpm for 5 min, and the supernatants were collected. Equal amounts of protein (20  $\mu$ g) were resolved by 10% SDS-PAGE and transferred onto PVDF membranes. Membranes were blocked with 5% BSA in PBS containing 0.05% Tween-20 (PBST) and incubated overnight at 4°C with primary antibodies diluted in the same buffer. After washing, membranes were incubated with HRP-conjugated secondary antibodies for 1 h at room temperature. Finally, the protein bands were detected using an enhanced chemiluminescence method.

### 2.3.6 Statistical analysis

All data were presented as mean  $\pm$  standard deviation (SD) using GraphPad Prism software (version 5.0; GraphPad Software Inc. San Diego, CA, USA). The experiments were performed in triplicate. Statistical analysis of the differences was determined using one-way ANOVA, followed by Tukey post hoc analysis at a significant level of  $p < 0.01$ .



Scheme 2. Synthesis route of pyranocoumarin derivatives (C01-C12).

## 2.4 Molecular docking study

Molecular docking studies were performed for the selected active compounds using AutoDock Vina version 1.2.7 integrated with the PyRx virtual screening tool (version 0.8). The crystal structure of the target protein COX-2 (PDB ID: 1CX2) was obtained from the RCSB Protein Data Bank (<https://www.rcsb.org/>). Protein preparation was carried out using Discovery Studio by removing water molecules, ions, and non-essential ligands, followed by adjustment of protonation states to reflect physiological pH. Ligand and receptor files were converted into PDBQT format using AutoDock Tools (version 1.5.7). The three-dimensional structures of the ligands were generated using ChemDraw, converted into PDB format, and energy-minimized to obtain stable conformations prior to docking. Docking simulations were conducted with an exhaustiveness value of 64, using a grid box encompassing the entire protein surface. For each docking run, eight binding poses were generated, and the conformation with the lowest binding energy was selected as the most favorable pose. Ligand-protein interactions were analyzed and visualized in both 2D and 3D formats using Discovery Studio Visualizer 2025. To validate the docking protocol, re-docking of the native co-crystallized ligand into its binding site was performed for each target protein, and the predicted pose was compared with the crystallographic pose by calculating the root-mean-square deviation (RMSD). Additionally, known drugs and inhibitors were docked into the target proteins as reference ligands for comparison with the test compounds (Rudrappa et al., 2023).

## 3. Results and Discussion

### 3.1 Synthesis of pyran-annulated derivatives

The target compounds were successfully synthesized via multi-component reactions (Schemes 1 and 2), affording moderate to good yields ranging from 48% to 87%. Pyranopyrazole derivatives were prepared through a one-pot, stepwise approach. In the first step, hydrazine hydrate or phenylhydrazine hydrate was reacted with ethyl acetoacetate under solvent-free conditions at room temperature to yield 3-methylpyrazol-5(4H)-one or 3-methyl-1-phenylpyrazol-5(4H)-one intermediates. These intermediates were subsequently condensed with malononitrile, aromatic aldehydes, and a catalytic amount of DMAP in ethanol under reflux for 1-2 h. In contrast, pyranocoumarin derivatives were obtained in a one-pot reaction of 4-hydroxycoumarin, malononitrile, and various aromatic aldehydes in the presence of catalytic DMAP, using ethanol as the solvent.

Overall, the N-phenyl-substituted pyranopyrazole derivatives (A01-A16) exhibited lower yields than their unsubstituted counterparts

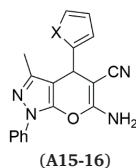
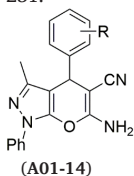
(B01-B16) and the pyranocoumarin derivatives (C01-C12). This reduction in yield may be attributed to the decreased nucleophilicity of the phenylhydrazine moiety, which could hinder the Knoevenagel condensation and subsequent C-H activation. In contrast, coumarin-derived pyrans were obtained in higher yields, likely due to the high nucleophilicity at the C-3 of coumarin, enhanced by the electron-withdrawing carbonyl at C-2 and the hydroxyl at C-4, which facilitates nucleophilic attack (Mohammadi Ziarani et al., 2019).

### 3.2 Effect of synthesized compounds on NO production in LPS-stimulated macrophage

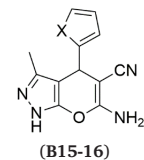
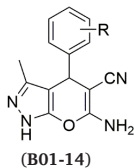
The anti-inflammatory potential of the synthesized compounds was evaluated based on NO inhibition in LPS-stimulated J774A.1 macrophages. Cytotoxicity was assessed prior to the assay, and only compounds exhibiting >80% cell viability at 50  $\mu$ M were selected for NO inhibition studies (Tables 1-2). Overall, N-phenylpyranopyrazoles

**Table 1.**

NO (J774A.1) and melanin (B16F10) inhibitory effect of compounds (A01-A16, B01-B16, C01-C12), and the cytotoxicity towards cancer cell MDA-MB-231.



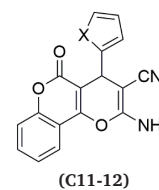
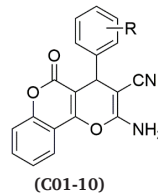
| Compound | R                       | X | IC <sub>50</sub> ( $\mu$ M) <sup>a</sup> |                |                |
|----------|-------------------------|---|--|----------------|----------------|
|          |                         |   | J774A.1                                  | B16F10         | MDA-MB-231     |
| A01      | H                       |   | >50                                      | 42.6 $\pm$ 1.7 | >50            |
| A02      | 3-OH                    |   | 21.2 $\pm$ 1.3                           | 37.9 $\pm$ 1.7 | >50            |
| A03      | 4-OH                    |   | 32.2 $\pm$ 1.5                           | >50            | >50            |
| A04      | 3-NO <sub>2</sub>       |   | 31.4 $\pm$ 1.5                           | 35.1 $\pm$ 1.5 | >50            |
| A05      | 4-NO <sub>2</sub>       |   | 10.2 $\pm$ 1.0                           | 13.3 $\pm$ 1.0 | 24.3 $\pm$ 1.2 |
| A06      | 3-OCH <sub>3</sub>      |   | 17.5 $\pm$ 1.2                           | 33.7 $\pm$ 1.3 | >50            |
| A07      | 4-OCH <sub>3</sub>      |   | 25.7 $\pm$ 1.4                           | >50            | >50            |
| A08      | 2,3-di OCH <sub>3</sub> |   | 16.5 $\pm$ 1.2                           | >50            | 45.1 $\pm$ 1.5 |
| A09      | 2,4-di OCH <sub>3</sub> |   | 45.1 $\pm$ 1.6                           | >50            | >50            |
| A10      | 4-OCF <sub>3</sub>      |   | 24.3 $\pm$ 1.5                           | 19.2 $\pm$ 1.4 | >50            |
| A11      | 4-F                     |   | 27.8 $\pm$ 1.4                           | 22.4 $\pm$ 1.1 | >50            |
| A12      | 3-Cl                    |   | 19.8 $\pm$ 1.2                           | 45.2 $\pm$ 1.3 | >50            |
| A13      | 4-Cl                    |   | 26.2 $\pm$ 1.4                           | 31.7 $\pm$ 1.6 | >50            |
| A14      | 4-Br                    |   | 46.8 $\pm$ 1.6                           | >50            | >50            |
| A15      |                         | S | 22.7 $\pm$ 1.3                           | >50            | >50            |
| A16      |                         | O | 12.4 $\pm$ 1.1                           | 32.7 $\pm$ 1.2 | 36.8 $\pm$ 1.3 |



| Compound | R                  | X | IC <sub>50</sub> ( $\mu$ M) <sup>a</sup> |        |            |
|----------|--------------------|---|--|--------|------------|
|          |                    |   | J774A.1                                  | B16F10 | MDA-MB-231 |
| B01      | H                  |   | >50                                      | >50    | >50        |
| B02      | 3-OH               |   | 34.3 $\pm$ 1.5                           | >50    | >50        |
| B03      | 4-OH               |   | 45.8 $\pm$ 1.6                           | >50    | >50        |
| B04      | 3-NO <sub>2</sub>  |   | 49.8 $\pm$ 1.5                           | >50    | >50        |
| B05      | 4-NO <sub>2</sub>  |   | 38.4 $\pm$ 1.5                           | >50    | >50        |
| B06      | 3-OCH <sub>3</sub> |   | 34.2 $\pm$ 1.5                           | >50    | >50        |

(Contd...)

| Compound | R                       | X | IC <sub>50</sub> ( $\mu$ M) <sup>a</sup> |                |                |
|----------|-------------------------|---|--|----------------|----------------|
|          |                         |   | J774A.1                                  | B16F10         | MDA-MB-231     |
| B07      | 4-OCH <sub>3</sub>      |   | 25.68 $\pm$ 1.2                          | >50            | 35.1 $\pm$ 1.2 |
| B08      | 2,3-di OCH <sub>3</sub> |   | >50                                      | >50            | >50            |
| B09      | 2,4-di OCH <sub>3</sub> |   | 40.11 $\pm$ 1.4                          | >50            | >50            |
| B10      | 4-OCF <sub>3</sub>      |   | 14.2 $\pm$ 1.1                           | 39.2 $\pm$ 1.6 | >50            |
| B11      | 4-F                     |   | 15.4 $\pm$ 1.1                           | >50            | 36.2 $\pm$ 1.3 |
| B12      | 3-Cl                    |   | 28.2 $\pm$ 1.4                           | >50            | >50            |
| B13      | 4-Cl                    |   | 17.2 $\pm$ 1.2                           | >50            | >50            |
| B14      | 4-Br                    |   | 17.4 $\pm$ 1.3                           | >50            | >50            |
| B15      |                         | S | >50                                      | >50            | >50            |
| B16      |                         | O | 20.7 $\pm$ 1.3                           | >50            | 31.2 $\pm$ 1.3 |



| Compound                  | R                  | X | IC <sub>50</sub> ( $\mu$ M) <sup>a</sup> |                |            |
|---------------------------|--------------------|---|--|----------------|------------|
|                           |                    |   | J774A.1                                  | B16F10         | MDA-MB-231 |
| C01                       | H                  |   | >50                                      | >50            | >50        |
| C02                       | 3-OH               |   | >50                                      | >50            | >50        |
| C03                       | 4-OH               |   | >50                                      | >50            | >50        |
| C04                       | 3-NO <sub>2</sub>  |   | 48.9 $\pm$ 1.6                           | >50            | >50        |
| C05                       | 4-NO <sub>2</sub>  |   | 27.1 $\pm$ 1.3                           | 33.1 $\pm$ 1.2 | >50        |
| C06                       | 4-OCH <sub>3</sub> |   | 31.4 $\pm$ 1.2                           | >50            | >50        |
| C07                       | 4-OCF <sub>3</sub> |   | 44.0 $\pm$ 1.3                           | >50            | >50        |
| C08                       | 4-F                |   | >50                                      | >50            | >50        |
| C09                       | 4-Cl               |   | >50                                      | >50            | >50        |
| C10                       | 4-Br               |   | >50                                      | >50            | >50        |
| C11                       |                    | S | 36.4 $\pm$ 1.7                           | >50            | >50        |
| C12                       |                    | O | 34.8 $\pm$ 1.5                           | 45.2 $\pm$ 1.3 | >50        |
| Indomethacin <sup>b</sup> |                    |   |  | 44.5 $\pm$ 1.5 |            |

The IC<sub>50</sub> values have been represented as the means  $\pm$  SD (n = 3); <sup>a</sup>The IC50 values are represented as the means  $\pm$  SD (n = 3); <sup>b</sup>Positive control

**Table 2.**

Binding energies of ligands (A05, A10, celecoxib, and indomethacin) to COX-2 (PDB code:1CX2) and targeting residues of the binding site.

| Compound     | Binding free energy (kcal/mol) | Residues   |
|--------------|--------------------------------|--|
| A05          | -10.26                         | ALA156, CYS47, PRO153, CYS36, GLY135, ARG 44, GLU46  |
| A10          | -8.45                          | TYR 36, MET48, ALA156, ASN34, VAL155, CYS159   |
| Celecoxib    | -9.71                          | PRO154, VAL155, ALA156, ASN39, CYS36, CYS37, GLN461, TYR 130, PRO153, GLU465, CYS41, ARG44 |
| Indomethacin | -7.21                          | ASN581, HIS351, GLY354, GLN192, TYR355   |

demonstrated stronger NO inhibitory activity than their unsubstituted analogs and the pyranocoumarin derivatives. The presence of a phenyl group at the pyrazole nitrogen likely enhances hydrophobicity, improves cell permeability, and enables  $\pi$ - $\pi$  stacking interactions with aromatic residues in the protein binding site. These factors, together with possible steric effects that promote a favorable molecular conformation, may account for the increased potency.

Substituents on the C4-aryl ring markedly influenced activity. Electron-withdrawing groups (EWGs), particularly at the para position,

significantly enhanced NO inhibition. Compound A05, bearing a 4-nitro (4-NO<sub>2</sub>) substituent, exhibited the highest potency with an IC<sub>50</sub> of 10.2 μM, followed by A10 with a 4-OCF<sub>3</sub> group (IC<sub>50</sub> = 24.3 μM), both outperforming the control indomethacin (IC<sub>50</sub> = 44.5 μM). These findings suggest that strong para-EWGs may enhance electronic interactions with the target protein, stabilizing the ligand-protein complex and conversely, relocating the EWG to the meta-position (C04, 3-NO<sub>2</sub>, IC<sub>50</sub> = 31.4 μM) reduced activity, underscoring the importance of substitution position for optimal binding.

Electron-donating groups (EDGs) at the meta position, such as methoxy (A06, IC<sub>50</sub> = 17.5 μM) and hydroxyl (A02, IC<sub>50</sub> = 21.2 μM), conferred moderate activity. The methoxy group outperformed the hydroxyl group, likely due to its greater lipophilicity, which could enhance cellular uptake and hydrophobic interaction within the binding pocket. In contrast, the polar hydroxyl group may engage in less favorable interactions or incur desolvation penalties. A disubstitution pattern with 2,3-dimethoxy groups (A08) exhibited higher potency than the 2,4-dimethoxy analogs (A09), suggesting that meta-oriented EDGs play a more critical role in enhancing activity.

Halogen substitutions also modulated activity. Fluorine-containing derivatives (A11, B11) displayed moderate potency, potentially due to the small size, and electronegativity of fluorine, which can enhance lipophilicity and metabolic stability. Bulkier halogens like bromine (A14, B14) slightly reduced activity, possibly due to steric hindrance.

Replacing the C-4 phenyl ring with a five-membered heteroaromatic ring also affected NO inhibitory activity of the compounds. A furan-substituted derivative (A16) displayed notable potency (IC<sub>50</sub> = 12.4 μM) likely due to its favorable electronic properties and the presence of the oxygen. Furan, which can participate in hydrogen bonding and dipole-dipole interactions. In contrast, thiophene substitution appeared less favorable, possibly due to the larger size of sulfur and increased electron delocalization, which may introduce steric hindrance.

Compared to the pyranopyrazole series, the coumarin-based derivatives (C-series) showed generally lower NO inhibitory activity. The rigid, planar, and sterically constrained coumarin scaffold may limit conformational adaptability within the binding site, reducing binding efficacy relative to the more flexible pyrazole-based framework.

### 3.2.1 Inhibitory effect of pyrano[2,3-c]pyrazole A05 on LPS-induced proteins and COX-2 expression

During the inflammation process, macrophages release mediators such as NO and pro-inflammatory cytokines, including interleukin-6 (IL-6), tumor necrosis factor-alpha (TNF-α), interleukin-1 beta (IL-1β), and prostaglandins, to facilitate tissue repair (Sharma et al., 2020; Wang et al., 2020). Non-steroidal anti-inflammatory drugs (NSAIDs)

are commonly used to inhibit cyclooxygenase (COX), which catalyzes the conversion of arachidonic acid into prostaglandins. COX exists in two isoforms: COX-1, which maintains renal and gastric function as well as vascular homeostasis, and COX-2, which mediates inflammatory responses (Ambatkar et al., 2023). Overexpression of COX-2 has been linked to increased BCL-2 expression and resistance to doxorubicin in cancer cells (Singh et al., 2008), underscoring COX-2 as a promising target for developing anti-inflammatory and anti-cancer agents.

To elucidate the molecular mechanism underlying the anti-inflammatory effect of A05, Western blot analysis was performed to assess its effect on the expression of inducible NO synthase (iNOS), COX-2, and TNF-α. As shown in Fig. 1, A05 treatment resulted in a concentration-dependent downregulation of iNOS and COX-2, with approximately 50% reduction at 10 and 25 μM, and complete suppression at 40 μM, reaching levels comparable to unstimulated cells. TNF-α expression, which was markedly increased by LPS stimulation, was also strongly suppressed by A05, with expression at 40 μM falling below basal levels observed in unstimulated controls, indicating potent inhibitory activity.

### 3.2.2 Molecular docking study with COX-2

Given the potent activity of A05 observed in both biochemical and cellular assays, molecular docking was carried out to further investigate its interaction with COX-2, a key inflammatory mediator. Docking simulations were performed alongside reference compounds celecoxib (a selective COX-2 inhibitor) and indomethacin (a non-selective NSAID) for comparison (Fig. 2; Table 2). The docking results revealed that A05 occupied the same active site as celecoxib within the COX-2 binding pocket, whereas indomethacin bound at a distinct site. A05 exhibited the lowest binding free energy (-10.26 kcal/mol) compared to A10 (-8.45 kcal/mol), celecoxib (-9.71 kcal/mol), and indomethacin (-7.21 kcal/mol). Although celecoxib interacted with a larger number of residues (11), A05 achieved a stronger binding energy through fewer but more energetically favorable interactions (6 residues), indicating a highly efficient binding mode. These findings align with the *in vitro* results and support the hypothesis that A05 may act as a selective COX-2 inhibitor, thereby contributing to its anti-inflammatory activity.

### 3.3 Effect of synthesized compounds on melanin production in B16F10 melanoma cells

Given the close relation between inflammation and melanogenesis, we extended our investigation to assess the anti-melanogenesis potential of the synthesized compounds. Inflammatory responses stimulate melanogenesis by upregulating pro-inflammatory mediators,

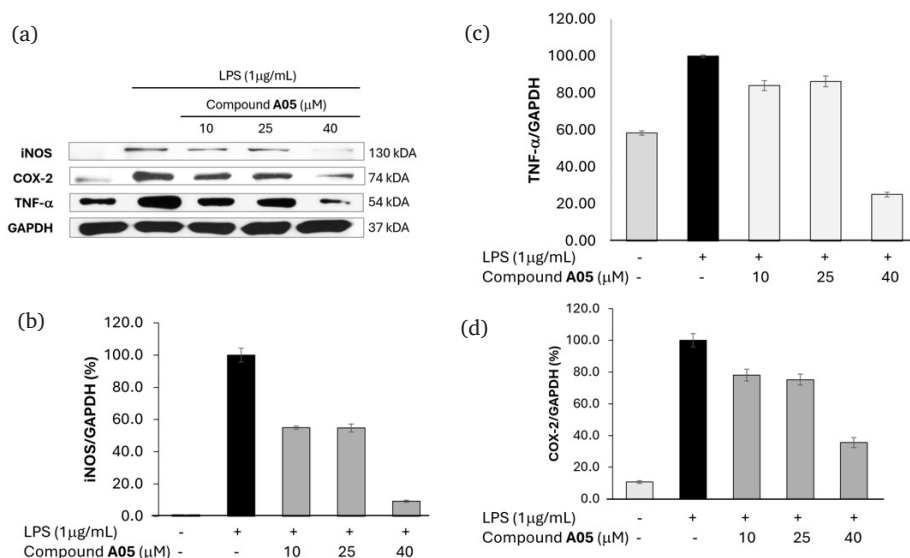


Fig. 1. (a) Western blot analysis showed the effect of A05 treatment on the expression of inflammatory mediators in LPS-stimulated J774A.1 macrophage cells, (b) COX-2, (c) iNOS, and (d) TNF-α.

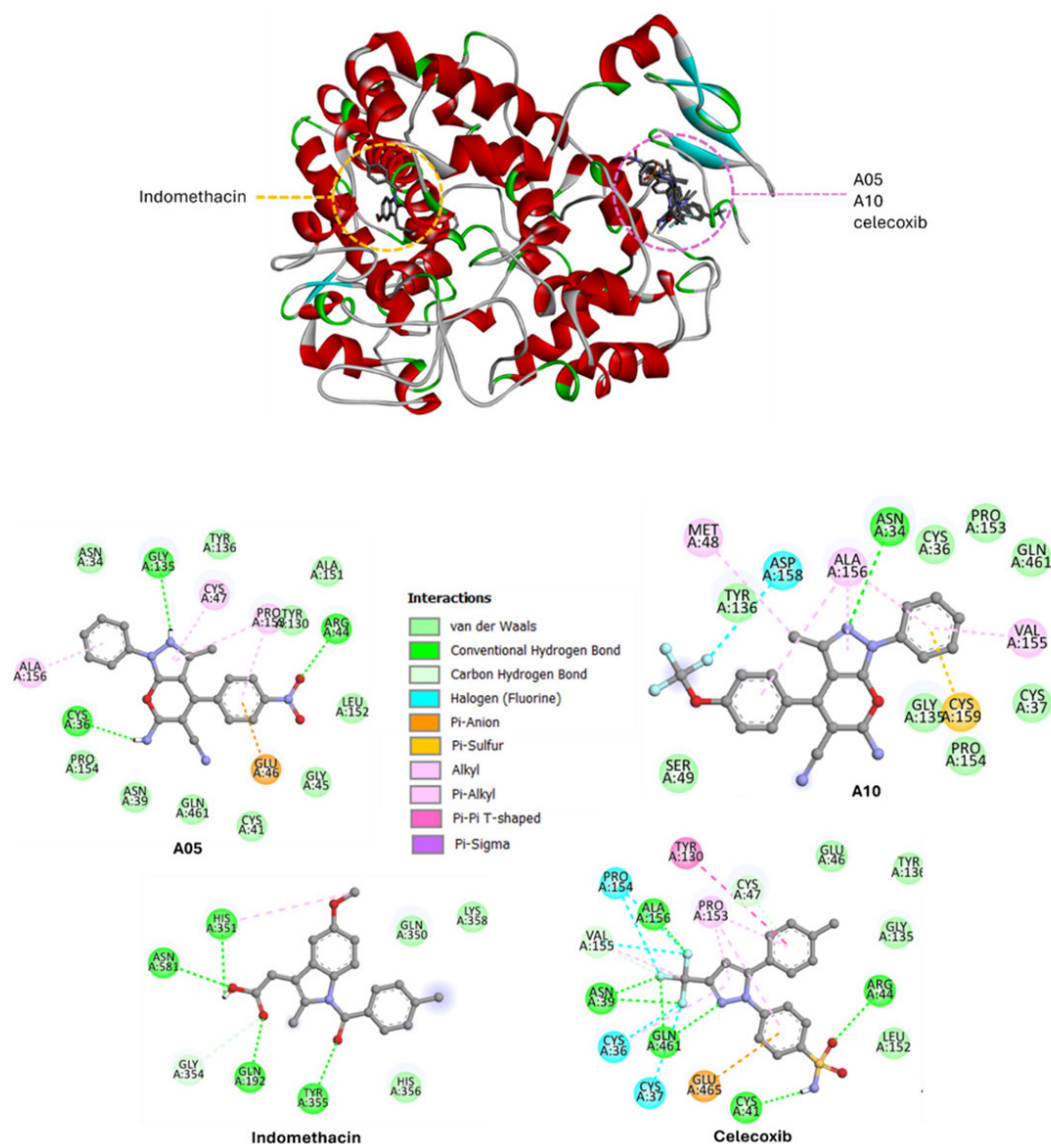


Fig. 2. The potential protein surface binding cavity in protein-ligand complex in 2D representation of interaction protein residues COX-2 (PDB ID: 1CX2) with compounds A05, A10, indomethacin, and celecoxib.

which activate melanocytes to produce melanin. Therefore, compounds with anti-inflammatory properties may also exhibit inhibitory effects on melanogenesis. Moreover, hyperpigmentation is a common adverse effect in patients undergoing chemotherapy or radiotherapy, further highlighting the therapeutic relevance of anti-melanogenesis agents.

Among all tested compounds, A05 displayed the strongest anti-melanogenic activity, with an  $IC_{50}$  value of 13.3  $\mu$ M. This activity was consistent with its anti-inflammatory effects. Compounds A10 and A11 also exhibited potent activity, with  $IC_{50}$  values of 19.2 and 22.4  $\mu$ M, respectively. Notably, these three compounds share a common structural feature: an EWG at the para-position of the phenyl ring. This suggests that para-substitution with EWGs may enhance interactions with melanogenesis-related proteins. By contrast, substitutions at the meta-position, regardless of electron-donating or electron-withdrawing nature, did not significantly influence activity, indicating a minimal role of meta-substitution in modulating melanogenesis inhibition.

Replacement of the pyrazole scaffold with a coumarin core, as in the C-series compounds, did not improve activity. The rigidity and planarity of the coumarin moiety may limit molecular flexibility and restrict binding to target proteins, thereby reducing inhibitory potential.

For comparison,  $\alpha$ -arbutin, a widely used cosmetic skin-whitening agent, was employed as a positive control. However,  $\alpha$ -arbutin exhibited only weak activity, requiring concentrations as high as 1000

$\mu$ M, and mild cytotoxicity was observed at this dose (Fig. 3). In contrast, A05 and A10 demonstrated significant anti-melanogenic activity at much lower concentrations without cytotoxicity, underscoring their potential as safer and more potent candidates. While A05 exhibited broad biological effects, including anti-inflammatory, anti-cancer, and anti-melanogenic activities, A10 selectively inhibited melanogenesis without notable effects in other assays. Based on this divergence in biological profiles, we investigated their molecular mechanisms using western blot analysis (Fig. 4).

Western blot results revealed that A10 treatment caused a concentration-dependent decrease in the expression of MITF, the master transcription factor regulating melanogenesis. However, substantial suppression of MITF was observed only at 50  $\mu$ M with minimal effect on TRP-1 at lower concentrations. In contrast, A05 strongly suppressed MITF expression even at lower concentrations. At 25  $\mu$ M, MITF expression was nearly abolished, and at 40  $\mu$ M, it was almost undetectable. TRP-1 expression was also markedly reduced in a dose-dependent manner. These findings indicate that A05 more effectively downregulates MITF than A10, which likely explains its superior anti-melanogenic activity. Since MITF controls downstream melanogenic enzymes, suppression by A05 may involve upstream regulation of multiple signaling pathways, including PI3K/Akt, MAPK/ERK, and CAMP/PKA/CREB (Jin et al., 2014). The limited reduction of

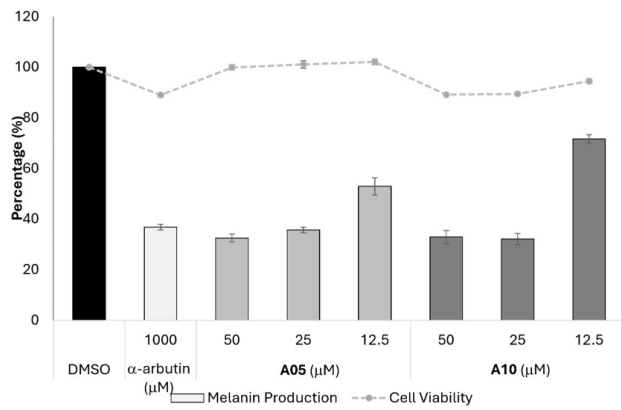


Fig. 3. Effects of A05, A10, and α-arbutin on melanin production and cell viability in B16F10 melanoma cells.

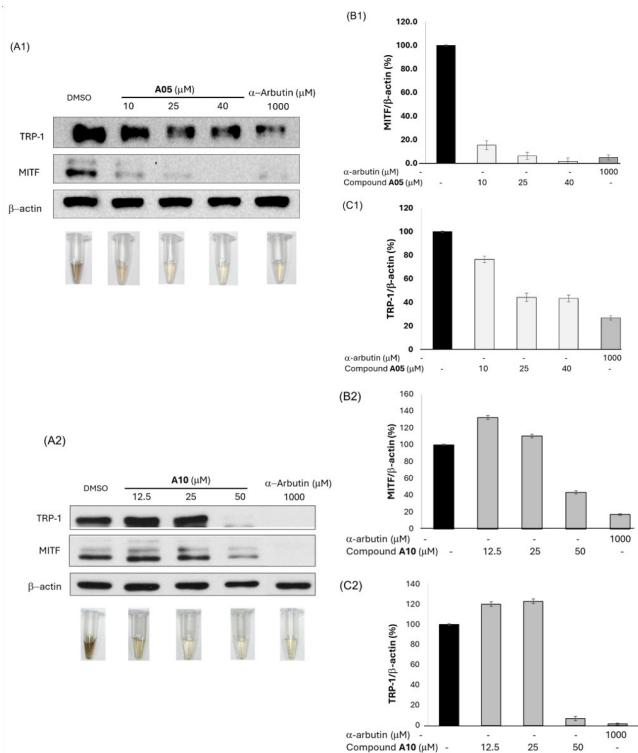


Fig. 4. Western blot analysis showed the effect of A05 (A1) and A10 (A2) treatment on the expression of inflammatory mediators in B16F10 (B1, B2) MITF and (C1, C2) TRP-1.

TRP-1 at lower concentrations further suggests that higher doses may be required to inhibit downstream melanogenesis proteins fully.

### 3.4 Effect of synthesized compounds on triple-negative MDA-MB-231 breast cancer cells

The synthesized compounds were further evaluated for cytotoxic activity against the MDA-MB-231 breast cancer cell line to explore the potential correlation between anti-inflammatory and anti-cancer properties. Chronic inflammation has been implicated in development and progression, particularly through the overexpression of pro-inflammatory mediators such as COX-2. MDA-MB-231, a triple-negative breast cancer (TNBC) line, is characterized by high COX-2 expression, making it a suitable *in vitro* model for investigating compounds with dual anti-inflammatory and anti-cancer potential (Basu et al., 2005).

The majority of compounds displayed weak cytotoxicity toward MDA-MB-231 cells ( $IC_{50} > 50 \mu M$ ). However, A05 emerged as a notable

exception, showing moderate cytotoxicity with an  $IC_{50}$  value of 24.3  $\mu M$ . Although this potency does not indicate strong cytotoxicity by conventional standards, A05 demonstrated a favorable selectivity profile, exhibiting no significant toxicity toward non-cancerous macrophage (J774A.1) and melanoma (B16F10) cells. This suggests that A05 may possess a therapeutically relevant safety margin, warranting further development.

Metastasis is a multistep process involving the dissemination of cancer cells from the primary tumor, invasion into surrounding tissues, intravasation into the circulation, and eventual colonization of distant organs (Lambert et al., 2017). Among these steps, cell migration plays a critical role in initiating invasion and metastasis. Given that, moreover, MDA-MB-231 cells are a highly invasive TNBC model with poor survival outcomes (Xu et al., 2024), inhibition of migration provides an important anti-metastatic potential.

The effect of A05 on cell migration was assessed using a wound-healing assay (Table 3; Fig. 5). Untreated control cells displayed high migratory capacity, with wound closure reaching approximately 80% after 48 h. In contrast, A05 treatment suppressed migration in a dose-dependent manner. At 6.25  $\mu M$ , a modest reduction in wound closure was observed. At 12.5  $\mu M$ , substantial inhibition was noted, while 25  $\mu M$  treatment resulted in near-complete suppression of wound closure, with minimal repair even after 48 h. At the highest concentration (50  $\mu M$ ), cell viability was severely compromised, reflecting cytotoxicity at twice the  $IC_{50}$  value. These findings indicate that A05 can effectively inhibit cancer cell motility at sub-cytotoxic concentrations, highlighting its potential as an anti-metastatic agent.

Collectively, the cytotoxicity and migration data suggest that the anti-cancer effects of A05 may be mediated not only through growth inhibition but also via interference with cellular processes critical to metastasis. Considering the established link between inflammation, COX-2 signaling, and cancer progression, the dual anti-inflammatory and anti-migratory effects of A05 underscore its promise as a multifunctional candidate for TNBC intervention.

Table 3.

The tissue repair percentage of MDA-MB-231 cells was treated with A05 at different concentrations and assessed by wound healing assay.

| Time (h) | Percentage of tissue repair (%) <sup>a</sup> |              |              |            |            |
|----------|--|--------------|--------------|------------|------------|
|          | Control                                      | 6.25 $\mu M$ | 12.5 $\mu M$ | 25 $\mu M$ | 50 $\mu M$ |
| 0        | 0.00   | 0.00         | 0.0          | 0.0        | 0.0        |
| 18       | 38.0   | 28.9         | 26.2         | 19.7       | 0.0        |
| 24       | 54.5   | 48.5         | 34.2         | 26.6       | 0.0        |
| 48       | 92.5   | 67.9         | 53.2         | 28.8       | 0.0        |

<sup>a</sup>Values have been expressed as mean (n = 2)

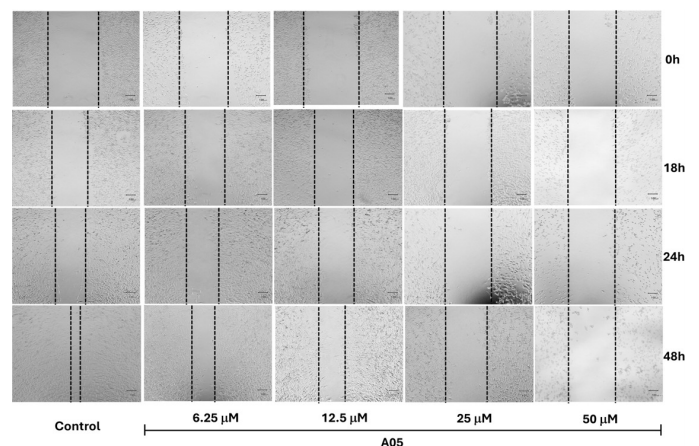


Fig. 5. Wound healing assay showed the effect of A05 on MDA-MB-231 cell migration at different concentrations over 0, 18, 24, and 48 h.

#### 4. Conclusions

The present study demonstrated that the synthesized compounds exhibit multiple and interconnected biological activities. In particular, **A05** emerged as the most promising candidate, displaying potent and consistent effects across anti-inflammatory, anti-melanogenesis, and anti-cancer assays. **A05** significantly inhibited NO production and downregulated the expression of iNOS, COX-2, and TNF- $\alpha$ , confirming its anti-inflammatory activity. Molecular docking further supported potential interactions with COX-2, providing a structural rationale for these effects. In parallel, **A05** effectively suppressed melanogenesis, primarily through downregulation of MITF and TRP-1, key regulators of melanin biosynthesis. Docking studies with MITF further reinforced this mechanism, suggesting that the anti-inflammatory and anti-melanogenic activities may be mechanistically linked. Beyond these effects, **A05** exhibited moderate cytotoxicity against TNBC cells while sparing non-cancerous cells, along with potent inhibition of cancer cell migration at sub-cytotoxic concentrations. These dual activities suggest that **A05** may modulate interconnected pathways involving inflammation, melanogenesis, and tumor progression. Significantly, **A05** did not induce phototoxicity, supporting its safety profile for potential therapeutic or cosmetic use.

Taken together, these findings highlight **A05** as a multifunctional scaffold with activity spanning anti-inflammatory, anti-melanogenic, anti-cancer, and anti-migratory effects. The convergence of these activities suggests a broader regulatory role in inflammation-driven disorders, pigmentation abnormalities, and cancer metastasis. Further studies should focus on elucidating the precise upstream signaling pathways (e.g., PI3K/Akt, MAPK/ERK, and cAMP/PKA/CREB), and optimized structural analogs to enhance potency and selectivity. Ultimately, the multifunctional nature of **A05** positions it as a promising lead compound for therapeutic development and cosmetic applications.

#### CRedit authorship contribution statement

**Dina Nur Shinta:** Concepts, design, literature search, experimental studies, data analysis, statistical analysis, manuscript preparation, manuscript editing and review. **Ardiansah Ardiansah:** Software, experimental studies (molecular docking). **Siwattra Choodej:** Manuscript editing and review. **Natthaya Chuaypen:** Methodology, resources (supporting). **Khanitha Pudhom:** Validation, reviewing and editing the manuscript, funding acquisition, project conceptualization, and supervision.

#### Declaration of competing interest

The authors declare that they have no competing financial interests or personal relationships that could have influenced the work presented in this paper.

#### Declaration of generative AI and AI-assisted technologies in the writing process

The authors confirm that there was no use of artificial intelligence (AI)-assisted technology for assisting in the writing or editing of the manuscript and no images were manipulated using AI.

#### Acknowledgement

This research project is supported by the Second Century Fund (C2F).

#### Supplementary data

Supplementary material is available at [https://dx.doi.org/10.25259/JKSUS\\_1363\\_2025](https://dx.doi.org/10.25259/JKSUS_1363_2025).

#### References

- Ahmad, A., Rao, S., Shetty, N.S., 2023. Green multi-component synthesis of pyrano[2,3-c]pyrazole derivatives: Current insights and future directions. *RSC Adv* 13, 28798-28833. <https://doi.org/10.1039/d3ra05570a>
- Ambatkar, M.P., Rarokar, N.R., Khedekar, P.B., 2023. Clinical Use of COX-2 Inhibitors containing quinoline heterocycle as a selective therapeutic agents for complementary medicine. *Clin Complementary Med Pharmacol* 3, 100102. <https://doi.org/10.1016/j.ccmp.2023.100102>
- Amirnejat, S., Nosrati, A., Peymanfar, R., Javanshir, S., 2020. Synthesis and anti-bacterial study of 2-amino-4H-pyrans and pyrans annulated heterocycles catalyzed by sulfated polysaccharide-coated BaFe<sub>3</sub>O<sub>19</sub> nanoparticles. *Res Chem Intermed* 46, 3683-3701. <https://doi.org/10.1007/s11164-020-04168-x>
- Bae, S., Hyun, C.G., 2023. The effects of 2'-hydroxy-3,6'-dimethoxychalcone on melanogenesis and inflammation. *IJMS* 24, 10393. <https://doi.org/10.3390/ijms241210393>
- Basu, G.D., Pathangey, L.B., Tindler, T.L., Gendler, S.J., Mukherjee, P., 2005. Mechanisms underlying the growth inhibitory effects of the cyclo-oxygenase-2 inhibitor celecoxib in human breast cancer cells. *Breast Cancer Res* 7. <https://doi.org/10.1186/bcr1019>
- Borges, F., Roleira, F., Milhazes, N., Santana, L., Uriarte, E., 2005. Simple coumarins and analogues in medicinal chemistry: occurrence, synthesis and biological activity. *CMC* 12, 887-916. <https://doi.org/10.2174/0929867053507315>
- Cao, Y., Yi, Y., Han, C., Shi, B., 2024. NF- $\kappa$ B signaling pathway in tumor microenvironment. *Front Immunol* 15. <https://doi.org/10.3389/fimmu.2024.1476030>
- Chaitanya Thandra, K., Barsouk, A., Saginala, K., Sukumar Aluru, J., Barsouk, A., 2021. Epidemiology of lung cancer. *WO* 25, 45-52. <https://doi.org/10.5114/wo.2021.103829>
- Cholayil Palapetta, S., Gurusamy, H., Ganapasam, S., 2023. Synthesis, characterization, computational studies, molecular docking, and *In Vitro* anti-cancer activity of dihydropyrano[3,2-c]chromene and 2-aminobenzochromene derivatives. *ACS Omega* 8, 7415-7429. <https://doi.org/10.1021/acso.3c00649>
- El-Sayed, N.N.E., Zaki, M.E.A., Al-Hussain, S.A., Ben Bacha, A., Berredjem, M., Masand, V.H., Almarhoon, Z.M., Omar, H.S., 2022. Synthesis and evaluation of some new 4H-pyran derivatives as anti-oxidant, anti-bacterial and anti-HCT-116 cells of CRC, with molecular docking, antiproliferative, apoptotic and ADME investigations. *Pharmaceuticals* 15, 891. <https://doi.org/10.3390/ph15070891>
- Fu, C., Chen, J., Lu, J., Yi, L., Tong, X., Kang, L., Pei, S., Ouyang, Y., Jiang, L., Ding, Y., Zhao, X., Li, S., Yang, Y., Huang, J., Zeng, Q., 2020. Roles of inflammation factors in melanogenesis (Review). *Mol Med Report* <https://doi.org/10.3892/mmr.2020.10950>
- Govindaiah, P., Dumala, N., Mattan, I., Grover, P., Jaya Prakash, M., 2019. Design, synthesis, biological and *in silico* evaluation of coumarin-hydrazone derivatives as tubulin targeted antiproliferative agents. *Bioorg Chem* 91, 103143. <https://doi.org/10.1016/j.bioorg.2019.103143>
- Jin, K.S., Oh, Y.N., Hyun, S.K., Kwon, H.J., Kim, B.W., 2014. Betulinic acid isolated from *Vitis amurensis* root inhibits 3-isobutyl-1-methylxanthine induced melanogenesis via the regulation of MEK/ERK and PI3K/Akt pathways in B16F10 cells. *Food Chem Toxicol* 68, 38-43. <https://doi.org/10.1016/j.fct.2014.03.001>
- Khare, S.P., Deshmukh, T.R., Akolkar, S.V., Sangshetti, J.N., Khedkar, V.M., Shingate, B.B., 2019. New 1,2,3-triazole-linked tetrahydrobenzo[b]pyran derivatives: Facile synthesis, biological evaluation and molecular docking study. *Res Chem Intermed* 45, 5159-5182. <https://doi.org/10.1007/s11164-019-03906-0>
- Kontogiorgis, C.A., Hadjipavlou-Litina, D.J., 2005. Synthesis and anti-inflammatory activity of coumarin derivatives. *J Med Chem* 48, 6400-6408. <https://doi.org/10.1021/jm0580149>
- Lambert, A.W., Pattabiraman, D.R., Weinberg, R.A., 2017. Emerging biological principles of metastasis. *Cell* 168, 670-691. <https://doi.org/10.1016/j.cell.2016.11.037>
- Lee, M.S., Chung, Y.C., Moon, S.H., Hyun, C.G., 2021. Lincomycin induces melanogenesis through the activation of MITF via p38 MAPK, AKT, and PKA signaling pathways. *JABC* 64, 323-331. <https://doi.org/10.3839/jabc.2021.044>
- Mohammadi Ziarani, G., Moradi, R., Ahmadi, T., Gholamzadeh, P., 2019. The molecular diversity scope of 4-hydroxycoumarin in the synthesis of heterocyclic compounds via multi-component reactions. *Mol Divers* 23, 1029-1064. <https://doi.org/10.1007/s11030-019-09918-7>
- Rajan, R.K., 2025. Piceatannol—Can it be used to treat hyperpigmentation of the Skin? *Pigment Cell Melanoma Res* 38. <https://doi.org/10.1111/pcmr.70008>
- Rudrappa, M., Nayaka, S., Kumar, R.S., 2023. In silico molecular docking approach of melanin against melanoma causing MITF proteins and anti-cancer, oxidation-Reduction, photoprotection, and drug-binding affinity properties of extracted melanin from *Streptomyces* sp. strain MR28. *Appl Biochem Biotechnol* 195, 4368-4386. <https://doi.org/10.1007/s12010-023-04358-4>
- Sharma, S., Kumar, D., Singh, G., Monga, V., Kumar, B., 2020. Recent advancements in the development of heterocyclic anti-inflammatory agents. *Eur J Med Chem* 200, 112438. <https://doi.org/10.1016/j.ejmech.2020.112438>
- Selvaraj, L., Eswaran, R., Natesan, V.K., Muthu, S.P., 2024. Tandem aqueous extract of onion catalyzed Knoevenagel condensation-Michael addition-cyclization: A green synthesis of 2-amino-3-cyano-4H-pyran derivatives and their anti-oxidant and molecular docking studies. *J Mol Struct* 1302, 137373. <https://doi.org/10.1016/j.molstruc.2023.137373>
- Shen, X., Hong, G., Wang, L., 2025. Recent advances in green multi-component reactions for heterocyclic compound construction. *Org Biomol Chem* 23, 2059-2078. <https://doi.org/10.1039/d4ob01822b>

- Singh, B., Cook, K.R., Vincent, L., Hall, C.S., Berry, J.A., Multani, A.S., Lucci, A., 2008. Cyclooxygenase-2 induces genomic instability, *BCL2* expression, doxorubicin resistance, and altered cancer-initiating cell phenotype in MCF7 breast cancer cells. *J Surg Res* 147, 240-246. <https://doi.org/10.1016/j.jss.2008.02.026>
- Stewart, Z.A., Westfall, M.D., Pietenpol, J.A., 2003. Cell-cycle dysregulation and anti-cancer therapy. *Trends Pharmacol Sci* 24, 139-145. [https://doi.org/10.1016/s0165-6147\(03\)00026-9](https://doi.org/10.1016/s0165-6147(03)00026-9)
- Sung, H., Ferlay, J., Siegel, R.L., Laversanne, M., Soerjomataram, I., Jemal, A., Bray, F., 2021. Global cancer statistics 2020: GLOBOCAN Estimates of Incidence and mortality worldwide for 36 cancers in 185 countries. *CA A Cancer J Clinicians* 71, 209-249. <https://doi.org/10.3322/caac.21660>
- Wang, L., Oh, J.Y., Jayawardena, T.U., Jeon, Y.J., Ryu, B.M.i, 2020. Anti-inflammatory and anti-melanogenesis activities of sulfated polysaccharides isolated from *Hizikia fusiforme*: Short communication. *Int J Biol Macromol* 142, 545-550. <https://doi.org/10.1016/j.ijbiomac.2019.09.128>
- Wang, Y.M., Wang, J.B., Huang, J., Cui, Z.S., Zhang, M., Zhang, Z.H., 2023. Molybdenum disulfide-catalyzed direct  $\alpha$ -hydroxymethylation of amides employing methanol as a sustainable C1 source under photoirradiation. *J Catal* 427, 115100. <https://doi.org/10.1016/j.jcat.2023.115100>
- Xu, G., Zhou, Q., Qi, J., Li, Z., Yin, L., Li, Z., Lu, C., Zhao, B., Shen, Y., 2024. Resveratrol-derived inhibitors of the E3 ubiquitin ligase PELI1 inhibit the metastasis of triple-negative breast cancer. *Eur J Med Chem* 265, 116060. <https://doi.org/10.1016/j.ejmech.2023.116060>